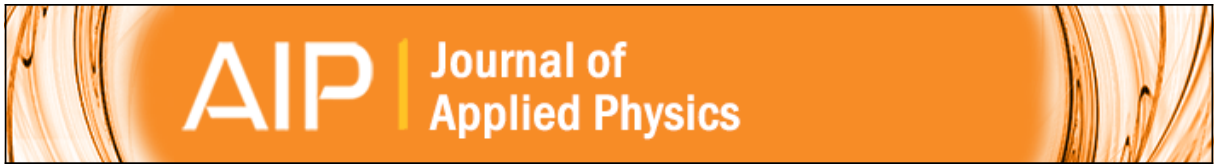


# Dynamic annealing in III-nitrides under ion bombardment

S. O. Kucheyev, J. S. Williams, J. Zou, and C. Jagadish

Citation: Journal of Applied Physics **95**, 3048 (2004); doi: 10.1063/1.1649459

View online: http://dx.doi.org/10.1063/1.1649459

View Table of Contents: http://scitation.aip.org/content/aip/journal/jap/95/6?ver=pdfcov

Published by the AIP Publishing



# Dynamic annealing in III-nitrides under ion bombardment

S. O. Kucheyev[a)]
*Research School of Physical Sciences and Engineering, The Australian National University, Canberra, ACT 0200, Australia and Lawrence Livermore National Laboratory, Livermore, California 94550*

J. S. Williams
*Research School of Physical Sciences and Engineering, The Australian National University, Canberra, ACT 0200, Australia*

J. Zou
*Division of Materials and Centre for Microscopy and Microanalysis, The University of Queensland, QLD 4072, Australia and Australian Key Centre for Microscopy and Microanalysis, The University of Sydney, NSW 2006, Australia*

C. Jagadish
*Department of Electronic Materials Engineering, Research School of Physical Sciences and Engineering, The Australian National University, Canberra, ACT 0200, Australia*

(Received 25 November 2003; accepted 19 December 2003)

We study the evolution of structural defects in $Al_xGa_{1-x}N$ films (with $x=0.0-0.6$) bombarded with kilo-electron-volt heavy ions at 77 and 300 K. We use a combination of Rutherford backscattering/channeling spectrometry and cross-sectional transmission electron microscopy. Results show that an increase in Al content not only strongly enhances dynamic annealing processes but can also change the main features of the amorphization behavior. In particular, the damage buildup behavior at 300 K is essentially similar for all the AlGaN films studied. Ion-beam-produced disorder at 300 K accumulates preferentially in the crystal bulk region up to a certain saturation level ($\sim$50%–60% relative disorder). Bombardment at 300 K above a critical fluence results in a rapid increase in damage from the saturation level up to complete disordering, with a buried amorphous layer nucleating in the crystal bulk. However, at 77 K, the saturation effect of lattice disorder in the bulk occurs only for $x \gtrsim 0.1$. Based on the analysis of these results for AlGaN and previously reported data for InGaN, we discuss physical mechanisms of the susceptibility of group-III nitrides to ion-beam-induced disordering and to the crystalline-to-amorphous phase transition.  [DOI: 10.1063/1.1649459]

## I. INTRODUCTION

Group-III nitrides (GaN, AlGaN, and InGaN) are important (opto)electronic materials. In the past several years, needs of the fast developing III-nitride technology have stimulated extensive studies of fundamental ion-beam-damage processes in GaN by a number of research groups. The current state of understanding of the defect evolution in GaN under keV ion bombardment can be found in several recent reviews on this topic.[1–4]

Recently, ion-bombardment-produced defects have also been studied in InGaN, AlGaN, and AlN.[5–14] It has been shown that an increase in In content strongly suppresses *dynamic annealing* processes (i.e., defect migration and interaction processes) and enhances the buildup of stable lattice disorder.[8] Interestingly, an increase in Al concentration in the AlGaN alloy has the opposite effect on the efficiency of dynamic annealing, increasing material resistance to ion-beam-induced disordering.[9,10] In this article, following our brief report,[9] we present a detailed study of the damage buildup behavior in $Al_xGa_{1-x}N$ films (with $x=0.0-0.6$) bombarded with kilo-electron-volt heavy ions at 77 and 300 K. We also compare the damage accumulation behavior in AlGaN with that previously reported for GaN,[1–4] InGaN,[8] and some other semiconductors. Emphasis is given to understanding physical processes responsible for the material resistance to ion-beam disordering and amorphization.

## II. EXPERIMENT

About 0.5-$\mu$m-thick $Al_xGa_{1-x}N$ films ($x=0.00$, 0.05, 0.08, 0.10, 0.13, 0.19, 0.40, and 0.60, with $\Delta x=0.02$, as assessed by Rutherford backscattering and x-ray diffraction) were used in this study. These AlGaN films were deposited by metal-organic chemical vapor deposition on the top of wurtzite undoped GaN epilayers grown on *c*-plane sapphire substrates. The deposition was done in two different EMCORE reactors at Ledex Corp. (Taiwan) and at EMCORE Corp. (Somerset, NJ). Samples were implanted with 300 keV $^{197}Au^+$ ions at 77 or 300 K with a beam flux of $\sim 3.1 \times 10^{12}\,cm^{-2}\,s^{-1}$ over the fluence range from $8\times10^{13}$ to $5\times10^{16}\,cm^{-2}$ using a 1.7 MV tandem accelerator (NEC, 5SDH-4) at the Australian National University. During implantation, samples were tilted by $\sim$7° relative to the incident ion beam to minimize channeling.

After implantation, all samples were characterized *ex situ* at 300 K by Rutherford backscattering/channeling spec-

a)Electronic mail: kucheyev1@llnl.gov

 

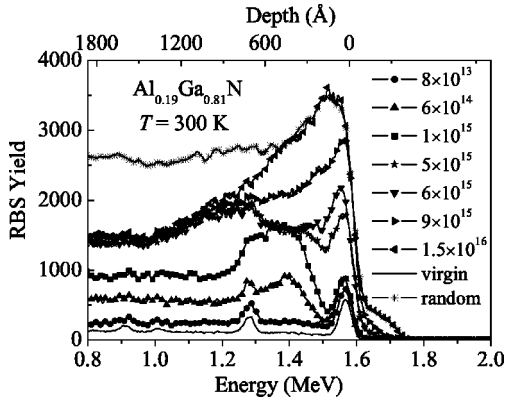


FIG. 1. Selected RBS/C spectra illustrating the buildup of structural disorder in $Al_{0.19}Ga_{0.81}N$ bombarded at 300 K with 300 keV Au ions with beam flux of $\sim 3.1\times10^{12}$ cm$^{-2}$ s$^{-1}$. Implantation fluences (in cm$^{-2}$) are indicated in the figure. The random spectrum is given for a fluence of $1.5\times10^{16}$ cm$^{-2}$.

trometry (RBS/C) using an ANU 1.7 MV tandem accelerator (NEC, 5SDH) with 1.8 MeV $^4He^+$ ions incident along the [0001] direction and backscattered into detectors at 98°, 115°, and 168° relative to the incident beam direction. The 8° glancing-angle detector geometry was used to provide enhanced depth resolution for examining near-surface damage accumulation. Scattering geometries with larger glancing angles were used to separate Au and Ga peaks in RBS/C spectra in samples implanted up to high Au fluences ($\geqslant 5\times10^{15}$ cm$^{-2}$). Note that all RBS/C spectra illustrated in this article were taken in the 8° glancing-angle detector geometry. All RBS/C spectra were analyzed using one of the conventional algorithms[15] for extracting depth-profiles of the effective number of scattering centers. For brevity, the number of scattering centers, normalized to the atomic concentration, will be referred to below as ''relative disorder.'' Selected samples were also studied by cross-sectional transmission electron microscopy (XTEM) in a Philips CM12 transmission electron microscope operating at 120 keV. XTEM specimens were prepared by 3 keV $Ar^+$ ion-beam thinning using a Gatan precision ion-polishing system.

## III. RESULTS

### A. Bombardment at 300 K

Figure 1 shows selected RBS/C spectra which illustrate the damage buildup in $Al_{0.19}Ga_{0.81}N$ films bombarded at 300 K with 300 keV Au ions. As briefly discussed in Ref. 9, the main features of the damage buildup behavior at 300 K illustrated in Fig. 1 are *common* for all the $Al_xGa_{1-x}N$ wafers studied (with $x = 0.05-0.60$). These features include (i) damage saturation in the crystal bulk close to the region of the maximum nuclear energy loss, (ii) the absence of preferential surface disordering and surface amorphization (in contrast to the case of $x = 0$; i.e., GaN), and (iii) a rapid increase in damage from the saturation level up to the random level, above a critical fluence.[16]

Preamorphous structural disorder in $Al_xGa_{1-x}N$ films (with $x = 0.08$ and 0.19) bombarded at 300 K to relatively small fluences of 300 keV Au ions has previously been studied by XTEM in Ref. 9. Hence, in the present study, we have examined by XTEM several AlGaN samples bombarded to high fluences when lattice amorphization is suggested by the RBS/C yield reaching the random level. For example, Fig. 2 shows that bombardment of $Al_{0.19}Ga_{0.81}N$ with 300 keV Au ions to a fluence of $1.5\times10^{16}$ cm$^{-2}$ results in the formation of a buried amorphous layer [compare bright- and dark-field images in Figs. 2(a) and 2(b)]. Figure 2 also illustrates the formation of planar defects which are parallel to the basal plane of the $Al_{0.19}Ga_{0.81}N$ film. Similar planar defects have previously been observed in GaN bombarded under a wide range of irradiation conditions[3,17,18] as well as in $Al_xGa_{1-x}N$ (with $x = 0.08$ and 0.19) and $In_{0.16}Ga_{0.84}N$ bombarded at 300 K with 300 keV Au ions to relatively low fluences.[8,9]

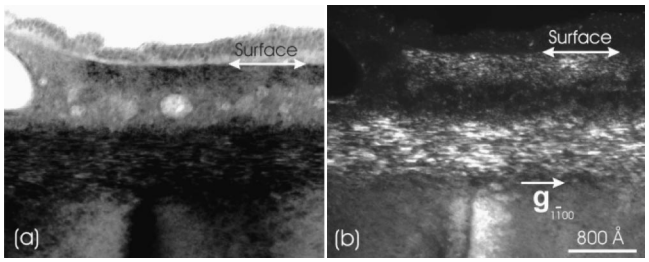


FIG. 2. Bright-field (a) and dark-field (b) XTEM images ($\mathbf{g} = 1\bar{1}00^*$) of $Al_{0.19}Ga_{0.81}N$ bombarded at 300 K with 300 keV Au ions with a beam flux of $\sim 3.1\times10^{12}$ cm$^{-2}$ s$^{-1}$ to a fluence of $1.5\times10^{16}$ cm$^{-2}$. Both images are of the same magnification and illustrate the same sample region. Note increased surface roughness of this sample due to the formation of circular inclusions within the buried amorphous layer.

Figure 2 also clearly illustrates a number of inclusions within the buried amorphous layer. The formation of similar close-to-circular inclusions has previously been observed by XTEM in GaN amorphized by ion bombardment.[19] This effect has been attributed to ion-beam-induced stoichiometric imbalance with the formation of $N_2$ gas bubbles[20] stimulated by the high plasticity of an amorphous phase of GaN.[21] Note that, for the sample from Fig. 2, surface exfoliation as a result of bubble growth, typically observed for GaN bombarded to high ion fluences, is hindered by a stiff surface layer of a crystalline material. Figure 2 strongly suggests that, similar to the case of GaN, $N_2$ bubble formation also occurs at 300 K in amorphous $Al_{0.19}Ga_{0.81}N$.

### B. Bombardment at 77 K

Our results have revealed that the damage buildup behavior in AlGaN at 77 K is more complex than that at 300 K. Figure 3 shows selected RBS/C spectra illustrating the damage accumulation in $Al_{0.05}Ga_{0.95}N$ films bombarded at 77 K with 300 keV Au ions. It is seen from Fig. 3 that, at 77 K, the main features of the damage buildup in $Al_{0.05}Ga_{0.95}N$ are similar to those in GaN, discussed in detail previously.[3,22] Indeed, Fig. 3 shows that, with increasing ion fluence, lattice damage gradually accumulates in the crystal bulk until the RBS/C yield reaches the random level for fluences above $\sim 10^{15}$ cm$^{-2}$, and the effect of damage saturation in the crystal bulk is not present. A qualitatively similar damage buildup behavior at 77 K has been observed for $Al_{0.08}Ga_{0.92}N$ films.

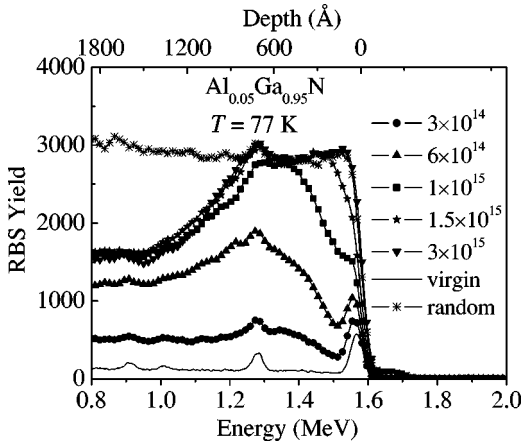


FIG. 3. Selected RBS/C spectra illustrating the buildup of structural disorder in $Al_{0.05}Ga_{0.95}N$ bombarded at 77 K with 300 keV Au ions with beam flux of $\sim 3.1\times10^{12}\,cm^{-2}\,s^{-1}$. Implantation fluences (in $cm^{-2}$) are indicated in the figure.

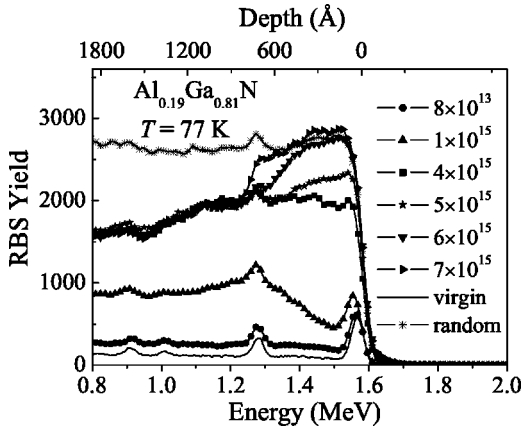


FIG. 5. Selected RBS/C spectra illustrating the buildup of structural disorder in $Al_{0.19}Ga_{0.81}N$ bombarded at 77 K with 300 keV Au ions with beam flux of $\sim 3.1\times10^{12}\,cm^{-2}\,s^{-1}$. Implantation fluences (in $cm^{-2}$) are indicated in the figure. The random spectrum is given for a fluence of $7\times10^{15}\,cm^{-2}$.

Figure 4 shows XTEM images of $Al_{0.05}Ga_{0.95}N$ bombarded at 77 K to a fluence of $1.5\times10^{15}\,cm^{-2}$, confirming the formation of a buried completely disordered (i.e., amorphous) layer, as suggested by RBS/C data from Fig. 3. Similar to the case of bombardment at 300 K discussed in the previous section, Fig. 4 reveals (i) no preferential surface disordering, (ii) the formation of planar defects parallel to the basal plane of the nitride film, and (iii) a number of inclusions in the buried amorphous layer, attributed to material decomposition with the formation of $N_2$ gas bubbles.

Our results show that an increase in Al content above ~0.1 changes the main features of the damage buildup behavior at 77 K. This is illustrated, for example, in Fig. 5, which shows selected RBS/C spectra representing the damage buildup in $Al_{0.19}Ga_{0.81}N$ films bombarded at 77 K. It is seen from Fig. 5 that, in contrast to the case of $Al_{0.05}Ga_{0.95}N$ shown in Figs. 3 and 4, the effect of defect saturation in the crystal bulk is observed. Note that the damage buildup behavior illustrated in Fig. 5 is common for all $Al_xGa_{1-x}N$ films with $x \gtrsim 0.1$ investigated in the present study. Hence, at 77 K, the damage buildup in $Al_xGa_{1-x}N$ with $x \gtrsim 0.1$ is qualitatively similar to that in $Al_xGa_{1-x}N$ (for all values of $x$ studied) at 300 K.

Figure 6 shows XTEM images of $Al_{0.19}Ga_{0.81}N$ bombarded at 77 K to a fluence of $7\times10^{15}\,cm^{-2}$, confirming the formation of an amorphous layer, as suggested by RBS/C data from Fig. 5. It is also seen from Fig. 6 that a thin ($\lesssim$100 Å) near-surface layer remains crystalline even after such relatively large fluence bombardment. This observation supports the fact that, in contrast to the case of GaN, the AlGaN surface is not a preferential site for amorphization. Rather, the surface of AlGaN appears to effectively promote defect annihilation.

## IV. DISCUSSION

### A. Damage buildup in AlGaN

Results presented herein show that both Al content and sample temperature strongly affect not only the level of ion-beam-produced preamorphous disorder but also the main features of the damage buildup behavior. The damage buildup behavior is better illustrated in Fig. 7, which summarizes defect accumulation curves at 300 K [Fig. 7(a)] and 77 K [Fig. 7(b)] for samples with different Al content. Shown in Fig. 7 are dependencies of relative disorder, extracted from RBS/C data, in the bulk defect peak region (~450 Å from the sample surface) as a function of displacements per atom (DPA). These DPA values are $N_{Ga}^{vac}\Phi/n_{Ga}^{at}$,

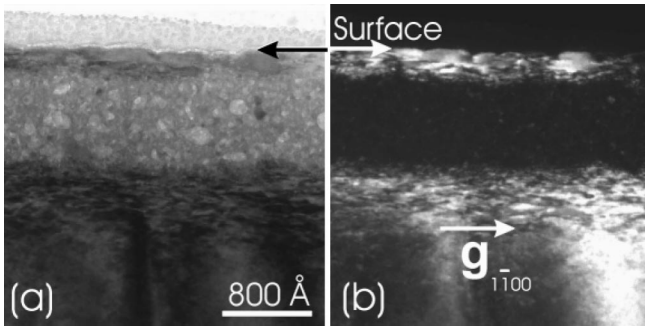


FIG. 4. Bright-field (a) and dark-field (b) XTEM images ($\mathbf{g}=1\bar{1}00^*$) of $Al_{0.05}Ga_{0.95}N$ bombarded at 77 K with 300 keV Au ions with a beam flux of $\sim 3.1\times10^{12}\,cm^{-2}\,s^{-1}$ to a fluence of $1.5\times10^{15}\,cm^{-2}$. Both images are of the same magnification.

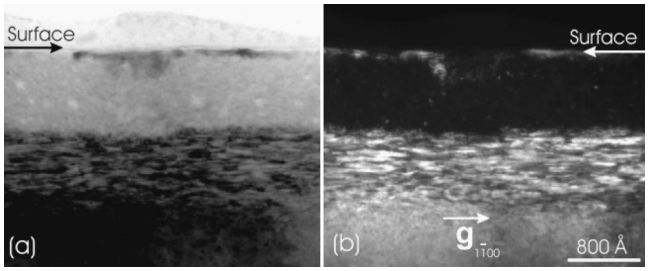


FIG. 6. Bright-field (a) and dark-field (b) XTEM images ($\mathbf{g}=1\bar{1}00^*$) of $Al_{0.19}Ga_{0.81}N$ bombarded at 77 K with 300 keV Au ions with a beam flux of $\sim 3.1\times10^{12}\,cm^{-2}\,s^{-1}$ to a fluence of $7\times10^{15}\,cm^{-2}$. Both images are of the same magnification.

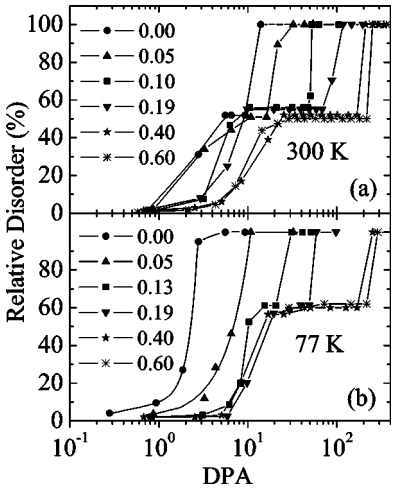


FIG. 7. Relative disorder (extracted from RBS/C spectra for the Ga peak) in the bulk defect peak region for $Al_xGa_{1-x}N$ samples as a function of displacements per atom (DPA). Samples were bombarded with 300 keV Au ions at 300 K (a) and 77 K (b) with a beam flux of $\sim 3.1\times 10^{12}\,cm^{-2}\,s^{-1}$. Aluminum content ($x$) in different samples is given in the legend.

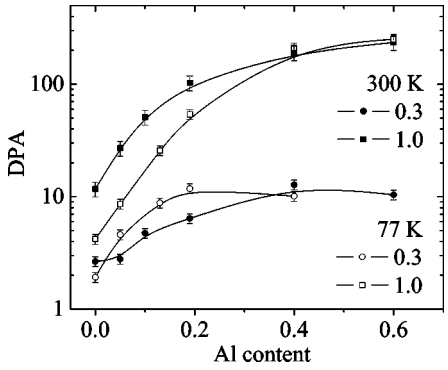


FIG. 8. Dependence of the displacements per atom (DPA) necessary to produce the level of relative lattice disorder of 30% ($DPA_{0.3}$) or 100% ($DPA_{1.0}$), as measured by RBS/C, on Al content ($x$) in the $Al_xGa_{1-x}N$ alloy bombarded with 300 keV Au ions with a beam flux of $\sim 3.1\times 10^{12}\,cm^{-2}\,s^{-1}$ at 77 or 300 K, as indicated in the legend. Lines are shown to guide the reader's eye.

where $N_{Ga}^{vac}$ is the average concentration of Ga vacancies generated by one ion per unit of depth in the bulk defect peak region, $n_{Ga}^{at}$ is the concentration of Ga atoms in the AlGaN alloy, and $\Phi$ is ion fluence. In order to estimate $N_{Ga}^{vac}$, ballistic simulations were performed with the TRIM code (version SRIM-2003.16)[23] with a threshold displacement energy of 25 eV for Al, Ga, and N atoms.[24] Such a conversion of ion fluences into DPA takes account of the difference in the number of atomic displacements ballistically generated by the ion beam in different AlGaN alloys. This allows the influence of factors other than the expected difference in ballistic processes to be studied. For DPA$\lesssim$0.3, when the lateral overlap of collision cascades is small, DPA values essentially indicate how many times each lattice atom has been *ballistically* displaced by the ion beam. For larger DPA values, however, it can be shown[25] that, in the absence of dynamic annealing (when all ion-beam-generated defects are essentially ''frozen'' in the lattice), the relative number of displaced atoms in the lattice accumulates as $1-\exp(-\mathrm{DPA})$, due to an effective lateral overlap of collision cascades produced by different ions.

Figure 7(a) illustrates that, for all values of $x$ at 300 K, defect saturation occurs at a relative disorder level of $\sim$50%–60%, and damage-DPA curves gradually shift toward larger DPA values with increasing $x$. For the case of bombardment at 77 K, Fig. 7(b) clearly illustrates a transition from the regime of a gradual damage buildup up to amorphization for $x\lesssim 0.1$ to the regime with saturation of damage in the bulk (at a disorder level of $\sim$60%) for $x\gtrsim 0.1$. The fact that the disorder level in the saturation regime is essentially independent of Al content and sample temperature (see Fig. 7) suggests that similar defect structures are present in $Al_xGa_{1-x}N$ in the saturation regime, when defect generation and dynamic annealing processes are effectively balanced.

The buildup of lattice disorder in semiconductors under ion bombardment can often be well fitted using defect overlap models.[25] However, we have not been able to find a satisfactory fit for damage buildup curves from Fig. 7 using simple disorder overlap models[25] for any values of the fitting parameters. This result is not unexpected since the damage buildup behavior in AlGaN is rather complex, involving effects such as (i) the formation of extended defects during ion bombardment, (ii) damage saturation in the crystal bulk, (iii) material decomposition, (iv) cascade density effects,[26] and (v) chemical effects of implanted species.[26] Thus, more sophisticated models need to be developed to qualitatively describe damage accumulation in materials with strong dynamic annealing.

The effect of Al content on the damage buildup is further illustrated in Fig. 8, which shows the values of DPA necessary to produce levels of relative disorder of 30% ($DPA_{0.3}$) and 100% ($DPA_{1.0}$) in the crystal bulk as a function of Al content $x$. A damage level of 30% corresponds to ion irradiation to fluences lower than those resulting in bulk damage saturation (at $\sim$50%–60%), while a disorder level of 100% obviously corresponds to the case of complete lattice disordering, as monitored by the ion channeling technique. Hence, $DPA_{0.3}$ indicates the efficiency of the formation of stable preamorphous disorder, whereas $DPA_{1.0}$ shows the ease of material amorphization. Note that, in the case of no dynamic annealing, $DPA_{0.3}$ and $DPA_{1.0}$ would be $\sim$0.3 and $\sim$3, respectively, independent of Al content.[27,28] Figure 8, however, reveals much larger values of $DPA_{0.3}$ and $DPA_{1.0}$, reflecting rather efficient dynamic annealing which increases with increasing Al content.

Figure 8 further reveals that a crystalline-to-amorphous transition occurs at smaller DPA values at 77 K as compared to that at 300 K. This result is consistent with the expected increase in the efficiency of defect annihilation processes with increasing sample temperature, which is typically observed in semiconductors.[29] Interestingly, Fig. 8 also shows that, an increase in irradiation temperature from 77 up to 300 K results in an *increase* in the amount of ion-beam-produced preamorphous disorder (i.e., a decrease in $DPA_{0.3}$). Hence, for relatively low levels of lattice disorder, such as 30%, an increase in dynamic annealing, with increasing sample temperature, results in the formation of energetically favorable

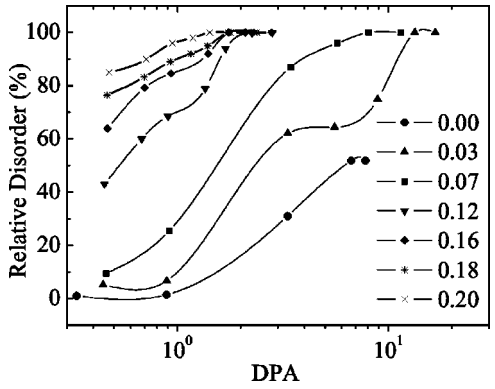


FIG. 9. Relative disorder (extracted from RBS/C spectra for the Ga peak) in the bulk defect peak region for $In_xGa_{1-x}N$ samples as a function of displacements per atom (DPA). Samples were bombarded with 300 keV Au ions at 300 K with a beam flux of $\sim 3.1\times10^{12}\,cm^{-2}\,s^{-1}$. Indium content ($x$) in different samples is given in the legend. Lines are shown to guide the reader's eye.

defect structures leading to a more efficient direct scattering of the analyzing $^4He^+$ particles. Thus, an increase in irradiation temperature from 77 up to 300 K results in an increase in the concentration of residual defects and/or a change in the atomic configuration of ion-beam-produced stable lattice defects. Additional systematic studies are, however, needed to better understand the physical mechanisms of such an increase in the defect level in AlGaN with increasing irradiation temperature.

### B. Damage buildup in InGaN

Before discussing the effect of Al and In content on dynamic annealing in group-III nitrides in the next section, we re-examine the damage buildup behavior in InGaN, based on experimental data from Ref. 8. In Ref. 8, $In_xGa_{1-x}N$ films (with $x=0.00$, 0.03, 0.07, 0.12, 0.16, 0.18, and 0.20) bombarded at 300 K with 300 keV Au ions with a beam flux of $\sim 3.1\times10^{12}\,cm^{-2}\,s^{-1}$ were studied by a combination of RBS/C and XTEM. Figure 9 shows damage buildup curves in InGaN films with different In concentrations replotted from Ref. 8 as a function of DPA. Similar to the case of AlGaN discussed in the previous section, such a conversion of ion fluences to DPA takes into account the difference in ballistic processes in different InGaN alloys. It is seen from Fig. 9 that an increase in In content suppresses dynamic annealing processes and weakens the effect of damage saturation (at the depth of the bulk disorder peak).

### C. Effect of Al and In content on dynamic annealing and amorphization

In this section, we discuss possible physical mechanisms controlling changes in the buildup of preamorphous lattice disorder and in amorphization of III-nitrides with variations in Al or In content.

#### 1. Preamorphous disorder

Results presented above have shown that adding Al increases (while adding In decreases) the level of dynamic annealing in AlGaN (and InGaN) ternary alloys. This result can be attributed to a larger (smaller) energy of the Al–N (In–N) bond as compared to the energy of the Ga–N bond (see Table I). Indeed, the buildup of preamorphous disorder in III-nitrides is associated with the formation of lattice defects involving broken and reconstructed bonds. It is expected that dynamic annealing processes, including defect annihilation, will be more efficient in a system with a larger energy gain due to the recovery of broken, distorted, and nonstoichiometric bonds, which are ballistically generated by the ion beam.

This argument, based on the energies of chemical bonds, can also be applied to explain dynamic annealing in $Al_xGa_{1-x}As$ alloys (see Table I),[30–32] studied in detail previously.[33] It should be noted, however, that, although the efficiency of dynamic annealing in AlGaN, InGaN, and AlGaAs alloys scales with the energy of chemical bonds (or the melting point, which is typically proportional to the bond energy), variations in other parameters can also be responsible for changes in the damage buildup behavior. For example, activation energies for various defect migration and interaction processes (which are not well known in AlGaN and InGaN) can also dramatically affect damage accumulation. In addition, possible segregation of In and/or Al atoms during ion bombardment could influence the buildup of stable lattice disorder. Hence, although the bond energy gives a clear trend in the efficiency of dynamic annealing and the buildup of preamorphous disorder in a number of semiconductor systems such as AlGaN, InGaN, and AlGaAs, a better understanding of the physical mechanisms controlling dynamic annealing in these semiconductors will need to await more detailed data on defect migration and interaction processes.

#### 2. Crystalline-to-amorphous phase transition

It is interesting to consider the influence of Al or In content on the susceptibility to amorphization and on amorphization mechanisms in III-nitrides. In contrast to the case of dynamic annealing and the buildup of preamorphous disorder discussed above, the influence of material parameters

TABLE I. Some properties of wurtzite III-nitrides as well as GaAs and AlAs at 300 K. Taken from Refs. 30–32.

| | Units | GaN | AlN | InN | GaAs | AlAs |
|---|---|---|---|---|---|---|
| Density | $g/cm^3$ | 6.15 | 3.23 | 6.81 | 5.32 | 3.76 |
| Melting point | K | ~2773 | 3273 | 1373 | 1513 | 2129 |
| Cohesive energy | eV/atom | 8.96 | 11.54 | 7.72 | 6.52 | 7.56 |
| Phillips ionicity | | 0.500 | 0.499 | 0.578 | 0.310 | 0.274 |

on susceptibility to ion-beam-induced amorphization has been a subject of several previous studies.[34–43] The following criteria for material susceptibility to amorphization induced by ballistic ion-beam processes have been proposed: (i) bond type;[34,35] (ii) the ratio of crystallization temperature to the melting point;[35] (iii) structural connectivity;[38] (iv) enthalpy or free energy difference between crystalline and amorphous phases;[39] and (v) an empirical combination of several of these parameters.[37,40]

However, the structural connectivity criterion[38] cannot explain the difference in amorphization susceptibility since AlGaN and InGaN alloys have the same (wurtzite) crystal structure. In addition, a quantitative analysis based on (i) the ratio of the crystallization temperature to the melting point[35] or (ii) an enthalpy or free energy difference[39] is difficult because enthalpies, free energies, and crystallization temperatures for AlGaN and InGaN alloys are currently unknown. Finally, based on the bond type criterion,[35,36] ion-beam-induced amorphization should occur in solids with bond ionicities (as defined by Phillips[30]) $\leqslant 0.47$, whereas solids with ionicities of chemical bonds above 0.60 remain crystalline even after high-fluence ion bombardment. Materials with bond ionicities between 0.47 and 0.60 typically show varying structural stability under ion bombardment.[35,36] It should be noted that the physical mechanisms underlying the empirical bond type criterion[35] are not well understood. Nevertheless, it has been suggested that an increase in electrostatic energy associated with substitutional disorder as ionicity increases[35] and/or the rotational rigidity of covalent bonds[34] may underlie the ionicity criterion for amorphization. Large bond ionicity can also facilitate defect annihilation by electrostatically lowering energy barriers to defect interaction processes.

Table I shows that Phillips ionicities[30] of GaN, AlN, and InN all fall into the last category of materials (with ionicities between 0.47 and 0.60) which may or may not exhibit ion-beam-induced amorphization. Hence, none of the criteria previously proposed can be directly applied to predict amorphization susceptibility of the AlGaN and InGaN alloys. What then are the criteria for amorphization in these materials and what are the underlying mechanisms?

Experiments[10,41] show that ion bombardment can render GaN and InN amorphous, while AlN remains crystalline at 300 K even after large fluences of heavy ions. Physical mechanisms of surface and bulk amorphization in GaN have been discussed in detail in Refs. 26 and 44. Possible initiators for the crystalline-to-amorphous phase transition in GaN include: (i) the sample surface; (ii) point and planar defects; (iii) stoichiometric imbalance and material decomposition; (iv) excess of interstitials or vacancies; and (v) implanted impurities. For GaN, it is clear that even at liquid nitrogen temperature, strong dynamic annealing effectively suppresses amorphization. However, defect annihilation processes are not perfect, and lattice defects in GaN effectively accumulate with increasing ion fluence. For such imperfect dynamic annealing, defect clustering in the bulk and trapping of defects at the sample surface are crucial for amorphization. With increasing concentration of ion-beam-produced stable lattice defects in GaN, the free energy of the defective material may rise above that of the amorphous phase, resulting in a catastrophic collapse of the defective crystalline lattice into an amorphous phase.[41,45]

For heavy-ion bombardment of AlGaN and InGaN, results presented above show that the sample surface is not a nucleation site for amorphization. As discussed in the previous section, an increase in Al content in AlGaN results in a more efficient defect annihilation, attributed to a larger energy of the Al–N bond as compared to that of the Ga–N bond. In this case, the free energy of the defective material may remain lower than that of the amorphous phase even for large ion fluences, resulting in an effective suppression of the crystalline-to-amorphous phase transition. An increase in Al content may also result in a large increase in the free energy of the amorphous phase of AlGaN, thus prohibiting energetically unfavorable amorphization.

Conversely, an increase in In content in InGaN dramatically enhances defect agglomeration processes. Such an enhancement of damage accumulation may be attributed to the trapping of ion-beam-generated point defects at In atoms and/or less energetically favorable recovery of broken and distorted In–N bonds as compared to the recovery of Ga–N bonds. These processes, in addition to possible changes in the free energy of the amorphous phase of InGaN, may enhance local amorphization in InGaN as the free energy of the defective crystal lattice exceeds that of the amorphous phase. However, at this stage additional studies would be desirable to further clarify the mechanisms of the influence of Al and In content on the susceptibility of group-III-nitride semiconductors to the ion-beam-induced crystalline-to-amorphous phase transition.

## V. CONCLUSIONS

In conclusion, the influence of Al content on the buildup of structural damage in $Al_xGa_{1-x}N$ films (with $x = 0.0–0.6$) under kilo-electron-volt heavy-ion bombardment at 77 and 300 K has been studied by a combination of RBS/C and XTEM. We have also reexamined our previous RBS/C and XTEM data on ion-beam-produced structural defects in InGaN.[8] The main results of the present work can be summarized as follows.

(i) An increase in Al concentration strongly enhances dynamic annealing processes and, hence, suppresses the production of stable lattice disorder in AlGaN under ion bombardment at 77 or 300 K.

(ii) An increase in Al content above ~0.1 changes the main features of the damage buildup behavior at 77 K. In particular, the effect of damage saturation in the crystal bulk at 77 K has been observed for $Al_xGa_{1-x}N$ with $x \gtrsim 0.1$ but not for samples with $x \lesssim 0.1$.

(iii) The level of relative disorder (~50%–60%) during the defect saturation regime (when it occurs) in the crystal bulk is essentially independent of Al content ($x = 0.0–0.6$) or implantation temperature (from 77 to 300 K).

(iv) All AlGaN (with $x = 0.0–0.6$) and InGaN (with $x = 0.0–0.2$) wafers studied have exhibited no preferential surface disordering, indicating that the AlGaN or InGaN surface is not a preferential site for amorphization.

(v) XTEM has revealed similar defect structures (with the formation of planar defects parallel to the nitride film) in AlGaN bombarded at 77 or 300 K as compared to those in GaN and InGaN.

(vi) An increase in irradiation temperature from 77 up to 300 K results in an increase in the amount of ion-beam-produced preamorphous disorder in AlGaN. The effective amorphization fluence, however, increases with increasing irradiation temperature from 77 up 300 K.

(vii) Finally, physical mechanisms controlling the susceptibility of AlGaN and InGaN to ion-beam-induced disordering and to the crystalline-to-amorphous phase transition have been discussed. It has been assumed that the crystalline-to-amorphous phase transition occurs when the free energy of the defective material exceeds that of the amorphous phase. An increase (decrease) in dynamic annealing with increasing Al (In) content has been attributed to a larger (smaller) energy of the Al–N (In–N) bond as compared to the energy of the Ga–N bond.

## ACKNOWLEDGMENTS

The authors would like to thank G. Li and M. O. Manasreh for supplying some of the samples investigated in the present study. This research was supported in part by the Australian Research Council. Work at LLNL was performed under the auspices of the U.S. Department of Energy by the University of California, Lawrence Livermore National Laboratory under Contract No. W-7405-Eng-48.

[1] S. J. Pearton, J. C. Zolper, R. J. Shul, and F. Ren, J. Appl. Phys. **86**, 1 (1999).
[2] B. Rauschenbach, in *III-Nitride Semiconductors: Electrical, Structural and Defects Properties*, edited by M. O. Manasreh, Chap. 7 (Elsevier, Amsterdam, 2000).
[3] S. O. Kucheyev, J. S. Williams, and S. J. Pearton, Mater. Sci. Eng., R. **33**, 51 (2001).
[4] C. Ronning, E. P. Carlson, and R. F. Davis, Phys. Rep. **351**, 349 (2001).
[5] J. C. Zolper, S. J. Pearton, C. R. Abernathy, and C. B. Vartuli, Appl. Phys. Lett. **66**, 3042 (1995).
[6] C. B. Vartuli, S. J. Pearton, C. R. Abernathy, J. D. MacKenzie, and J. C. Zolper, J. Vac. Sci. Technol. B **13**, 2293 (1995).
[7] A. Y. Polyakov, M. Shin, M. Skowronski, R. G. Wilson, D. W. Greve, and S. J. Pearton, Solid-State Electron. **41**, 703 (1997).
[8] S. O. Kucheyev, J. S. Williams, J. Zou, S. J. Pearton, and Y. Nakagawa, Appl. Phys. Lett. **79**, 602 (2001).
[9] S. O. Kucheyev, J. S. Williams, J. Zou, G. Li, C. Jagadish, M. O. Manasreh, M. Pophristic, S. Guo, and I. T. Ferguson, Appl. Phys. Lett. **80**, 787 (2002).
[10] S. O. Kucheyev, J. S. Williams, J. Zou, C. Jagadish, M. Pophristic, S. Guo, I. T. Ferguson, and M. O. Manasreh, J. Appl. Phys. **92**, 3554 (2002).
[11] R. M. Frazier, G. T. Thaler, C. R. Abernathy, S. J. Pearton, M. L. Nakarmi, K. B. Nam, J. Y. Lin, H. X. Jiang, J. Kelly, R. Rairigh, A. F. Hebard, J. M. Zavada, and R. G. Wilson, J. Appl. Phys. **94**, 4956 (2003).
[12] R. M. Frazier, J. Stapleton, G. T. Thaler, C. R. Abernathy, S. J. Pearton, R. Rairigh, J. Kelly, A. F. Hebard, M. L. Nakarmi, K. B. Nam, J. Y. Lin, H. X. Jiang, J. M. Zavada, and R. G. Wilson, J. Appl. Phys. **94**, 1592 (2003).
[13] T. Oishi, N. Miura, M. Suita, T. Nanjo, Y. Abe, T. Ozeki, H. Ishikawa, T. Egawa, and T. Jimbo, J. Appl. Phys. **94**, 1662 (2003).
[14] F. Lu, H. Hu, and A. Rizzi, Appl. Surf. Sci. **205**, 262 (2003).
[15] K. Schmid, Radiat. Eff. **17**, 201 (1973).
[16] Note in Fig. 1 a pronounced increase in the RBS yield near the sample surface for Au fluences above $\sim 5\times 10^{15}\,\mathrm{cm}^{-2}$. Such an increase in the RBS yield for both channeling and random spectra is due to an overlap of Au and Ga peaks in the spectra taken with the 8°-glancing-angle scattering geometry.
[17] C. M. Wang, W. Jiang, W. J. Weber, and L. E. Thomas, J. Mater. Res. **17**, 2945 (2002).
[18] Y. G. Wang, J. Zou, S. O. Kucheyev, J. S. Williams, C. Jagadish, and G. Li, Electrochem. Solid-State Lett. **6**, G34 (2003).
[19] S. O. Kucheyev, J. S. Williams, C. Jagadish, V. S. J. Craig, and G. Li, Appl. Phys. Lett. **77**, 1455 (2000).
[20] S. O. Kucheyev, J. S. Williams, J. Zou, C. Jagadish, and G. Li, Appl. Phys. Lett. **77**, 3577 (2000).
[21] S. O. Kucheyev, J. E. Bradby, J. S. Williams, C. Jagadish, M. V. Swain, and G. Li, Appl. Phys. Lett. **78**, 156 (2001).
[22] S. O. Kucheyev, J. S. Williams, J. Zou, G. Li, C. Jagadish, and A. I. Titov, Nucl. Instrum. Methods Phys. Res. B **190**, 782 (2002).
[23] J. F. Ziegler, J. P. Biersack, and U. Littmark, *The Stopping and Range of Ions in Solids* (Pergamon, New York, 1985).
[24] To our knowledge, no experimental studies to determine the value of the threshold displacement energy ($E_d$) for Ga, Al, and N in AlGaN or InGaN have been reported in the literature. Hence, possible deviations of effective $E_d$ values from 25 eV, assumed in our simulations, can introduce some error, and the determination of $E_d$ for group-III nitrides requires additional studies.
[25] See, for example, a review by W. J. Weber, Nucl. Instrum. Methods Phys. Res. B **166–167**, 98 (2000).
[26] S. O. Kucheyev, J. S. Williams, C. Jagadish, J. Zou, G. Li, and A. I. Titov, Phys. Rev. B **64**, 035 202 (2002).
[27] It should be noted that, for ion bombardment conditions with suppressed dynamic annealing, lattice disorder often accumulates faster than as predicted by ballistic calculations such as the TRIM code.[23] This effect has been attributed to collective nonlinear processes in collision cascades.[28]
[28] See, for example, a review by D. A. Thompson, Radiat. Eff. **56**, 105 (1981).
[29] See, for example, a review by J. S. Williams, Rep. Prog. Phys. **49**, 491 (1986).
[30] J. C. Phillips, Rev. Mod. Phys. **42**, 317 (1970).
[31] W. A. Harrison, *Electronic Structure and the Properties of Solids* (Dover, New York, 1989).
[32] *CRC Handbook of Chemistry and Physics*, edited by D. R. Lide (CRC, Boca Raton, FL, 1992).
[33] See, for example, H. H. Tan, C. Jagadish, J. S. Williams, J. Zou, D. J. H. Cockayne, and A. Sikorski, J. Appl. Phys. **77**, 87 (1995); B. W. Lagow, I. M. Robertson, L. E. Rehn, P. M. Baldo, J. J. Coleman, and T. S. Yeoh, J. Mater. Res. **15**, 2043 (2000), and references therein.
[34] P. V. Pavlov, E. I. Zorin, D. I. Tetelbaum, V. P. Lesnikov, G. M. Ryzhkov, and A. V. Pavlov, Phys. Status Solidi A **19**, 373 (1973).
[35] H. M. Naguib and R. Kelly, Radiat. Eff. **25**, 1 (1975).
[36] Hj. Matzke, Radiat. Eff. **64**, 3 (1982).
[37] R. K. Eby, R. C. Ewing, and R. C. Birtcher, J. Mater. Res. **7**, 3080 (1992).
[38] L. W. Hobbs, A. N. Sreeram, C. E. Jesurum, and B. A. Berger, Nucl. Instrum. Methods Phys. Res. B **116**, 18 (1996).
[39] N. Q. Lam, P. R. Okamoto, and M. Li, J. Nucl. Mater. **251**, 89 (1997).
[40] S. X. Wang, L. M. Wang, R. C. Ewing, and R. H. Doremus, J. Non-Cryst. Solids **238**, 214 (1998); L. M. Wang, S. X. Wang, W. L. Gong, R. C. Ewing, and W. J. Weber, Mater. Sci. Eng., A **253**, 106 (1998).
[41] J. S. Williams, Mater. Sci. Eng., A **253**, 8 (1998).
[42] P. M. Ossi and R. Pastorelli, J. Appl. Phys. **85**, 1387 (1999).
[43] A. Meldrum, S. J. Zinkle, L. A. Boatner, and R. C. Ewing, Phys. Rev. B **59**, 3981 (1999).
[44] S. O. Kucheyev, J. S. Williams, C. Jagadish, J. Zou, and G. Li, Phys. Rev. B **62**, 7510 (2000).
[45] M. L. Swanson, J. R. Parsons, and C. W. Hoelke, Radiat. Eff. **9**, 249 (1971).